POLITECNICO
MILANO 1863

SCUOLA DI INGEGNERIA INDUSTRIALE
E DELL'INFORMAZIONE

Understanding the mismatch between clinical and numerical measurements of nasal resistance

Tesi di Laurea Magistrale in Ingegneria Aeronautica

Berkay Üçöz, 10817224

Abstract: There is a mismatch between clinical measurements of nasal resistance via rhinomanometry and results from Computational Fluid Dynamics (CFD). The discrepancy is often much larger than the accepted experimental or simulation uncertainties and the aim of the present work is identifying possible source of errors compatible with this mismatch. Results of a previous experimental campaign are compared against different numerical strategies, including both Reynolds-average Navier–Stokes simulations and Direct Numerical Simulations, on the same anatomical geometry. The setup of experiments and simulations is created to emulate that of an active anterior rhinomanometry. Of all considered sources of uncertainty, which include a lack of resolution, the intrinsic modelling approximations, and the usage of dissipative numerical schemes, we found that the largest one is that related to the position of pressure measurements in clinical instruments. It is also the only one compatible with the mismatch between clinical measurement and simulations. Our results suggest that a source of systematic bias may be present in rhinomanometers with a design similar to the instrument considered in our study. This bias could be the main culprit of the mismatch between clinical measurements and simulations results.

Advisor:
Prof. Maurizio Quadrio

Co-advisors:
Dr. Marco Atzori

Academic year:
2022-2023

Key-words: Nasal Resistance, Rhinomanometry, CFD

1. Introduction

The aim of the present work stems from the fact that there is a disagreement between measurements of nasal resistance via rhinomanometry and Computational Fluid Dynamics (CFD). The nasal resistance, defined as $R = \Delta P/Q$, is the ratio between pressure drop and corresponding flow rate through the nasal cavity during breathing, which are denoted respectively by ΔP and Q. In this context, the nasal cavity is the region of the upper airways starting from the nostrils and arriving up to the nasopharynx, where the two trackes that originate at the nostrils join together. The nasal resistance is a relevant quantity in the clinical practice because it plays a role in the diagnosis of nasal airway obstructions (NAOs). While not deadly, NAOs are nevertheless responsible for difficulties in breathing through the nose, often causing serious discomfort and negatively affecting the quality of life, and are a quite common condition [1].

The nasal resistance is typically measured through the exam know as *rhinomanometry* (RMM), which can be carried out with different methodologies. The Anterior Active Rhinomanometry (AAR) has become the most common, due its relatively simplicity and ease to carry out [2] (the AAR setup will be described in detail in the following section). The measured values of nasal resistance are one of the elements that is considered in planning surgery. However, it is known that rhinomanometry results are not robust and can be difficult to reproduce, since physiological modifications of the interior of the nasal cavity can cause significant variations of R. For instance, Thulesius [3] reported that when nasal resistance is inspected at regular intervals over a period, high nasal resistance change varying from normal levels to pathological ones or vice versa is observed. This fact, the complexity of the nasal cavity and their high anatomical variability, gave a high incentive for exploring numerical simulations as a complementary tool for the study of NAOs. CFD has been considered by a number of authors, including, recently, for aiding the planning of surgery. For instance, Berger *et al.* [4] used data obtained from Lattice-Boltzmann simulations for optimization of the geometry of the nasal airway. We refer to Quadrio *et al.* [5] and Radulesco *et al.* [6] for comprehensive reviews of these usage of numerical simulations in the study of airflow through the nasal cavity. We focus here on the fact that, while CFD simulations and rhinomanometry predicts similar trends, the values of nasal resistance between the two methods are often in disagreement.

Kimbell *et al.* [7] reported that the nasal resistance found with CFD simulations are lower than those the RMM measurements. The main objective of the study was to develop a comparison method for the CFD-derived nasal resistance and the patient-reported NAO. Another study conducted by Osman *et al.* [8] aimed at directly validate the CFD-derived nasal resistances

with RMM-measured ones. The authors found that CFD results were in general agreement with the RMM measurements of Vogt *et al.* [9], but still lead to a gross underestimation of nasal resistances. Berger *et al.* [10] reported that error rates up to 100% are observed between the nasal resistance of CFD simulations and AAR measurements, even though CFD simulations were validated with laser Doppler Anemometry (LDA) [11]. Lastly, Schmidt *et al.* [12], in the investigation of measurement uncertainties caused by RMM, confirmed significant differences between medical RMM and CFD simulation results.

Even though the order of magnitude of these discrepancies is larger than the uncertainties that could be expected from both numerical simulation and standard experimental measurements, the source of mismatch has not been systematically investigated yet. A natural suspect could be the reconstruction procedure that is necessary to obtain a geometry suitable for CFD codes from X-ray images or computed tomography (CT) scan (we refer *e.g.* to Waldmann *et al.* [13] for a description of the full workflow). Indeed, it has been found that a change of the anatomy compatible with a reasonable modification of the segmentation threshold in the reconstruction procedures can have a non-negligible impact on CFD results [14], but not large enough to be a satisfactory explanation for the mismatch between simulations and clinical measurements.

The present work is part of a larger effort devoted to improve our understanding of the physiology of the nasal cavity and to provide reliable CFD tools for the medical practice. On the one hand, Vecchietti [15] and Schillaci & Quadrio [16] already carried out a large set of numerical simulations on different anatomies, to establish a robust work flow for simulations of these cases. On the other hand, Tesa [17], created the experimental setup that is described in the following section, to reproduce the AAR procedure of an AAR using both a medical rhinomanometer and precise standard laboratory instruments. In this paper, a new numerical data set is created, with simulations of the same geometry used for the experiment in Ref. [17]. After describing the numerical and experimental setup in Section 2, we will carefully compare errors in numerical simulations with that related to a possible cause of bias in the design of medical rhinomanometers in Section 3, and finally summaries our findings in Section 4.

2. Methodology

In the present section, we describe the general framework of our study and the setup of simulations and experiments. A number of simplifications are adopted with respect to what would be necessary for capturing all aspects of human respiration. The flow through the nasal cavity is assumed to be incompressible and with constant density, so that the governing equations

are:

$$\nabla \cdot \mathbf{u} = 0 \tag{1}$$

$$\frac{\partial \mathbf{u}}{\partial t} + \mathbf{u} \cdot \nabla \mathbf{u} = -\frac{1}{\rho} \nabla p + \nu \nabla^2 \mathbf{u} \,. \tag{2}$$

In these expressions, $\mathbf{u}$ denotes the velocity vector, ν denotes the kinematic viscosity, ρ denotes the fluid density, and p denotes the pressure. Moreover, the average of the velocity field is denoted with $\overline{u}$ and the velocity fluctuation from the average value is denoted with u'. While heat transfer from the patient to the inspired air plays a role in the perception of respiration [18, 19], the relatively small velocity and temperature variations justify the incompressibility assumption from the point of view of taking into account the relevant flow dynamics [20]. In the present case, moreover, the silicon cast of the nasal cavity used in the experiment is approximately at ambient temperature.

In the clinical practice, a full inhalation-exaltation cycle is necessary for a proper assessment of the nasal resistance. In the present study, we focus on cases with a constant flow rate and only inspiration for both experiment and simulations. Interestingly, it has been argued that the assumption of constant flow rate is reasonable even for simulations aimed at reproducing the flow during actual respiration, as long as only inhalation or exhalation are considered [21].

The geometry selected for this study is a human nasal path reconstructed from a CT scan provided by the San Paolo Hospital, University of Milan. The same 3D model obtained from the scan was used as a base for the silicon cast created for the experiments by Tesa [17] and in our simulation. In both cases, the model is made in scale 2:1, to ease the casting procedure and experimental measurements. The portion of the respiratory track included in the model contains the nasal vestibule, nasal conchae, sinuses, and pharynx. The sampling technique used in the AAR, which will be explained in Section 2.1, requires to measure the nasal resistance separately for each side of the nasal cavity, while the nostril of the opposite side is sealed. In the experiment, the medical procedure is repeated to the letter and an appropriate sealing is applied. In the simulation, the 3D model is modified to the same effect. In the present study, we focus on results obtained with the left nostril sealed and right nostril active (note that left and right are referred to the doctor's perspective, assuming the doctor is in front of patient). Unfortunately, additional filling was required in the experimental setup to improve the adhesion of mask and silicon model, which was not possible to realistically reproduce in the simulation setup. Following the same strategy of previous studies, the computational domain in simulations is limited by a spherical surface where "far-field" boundary conditions are imposed [22, 10]. The modified geometry is shown in Fig. 1.

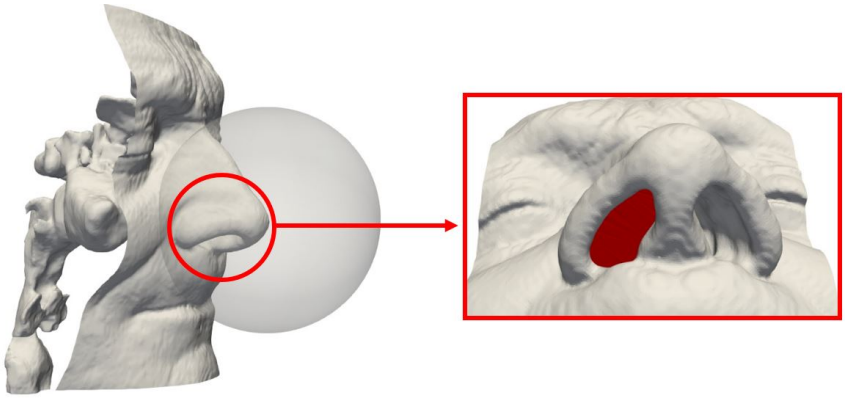

Figure 1: Modified geometry used to reproduce the typical setup of the Active Anterior Rhinomanometry.

2.1. Experiment Setup

The experimental data set used in this work is part of a larger one created by Tesa [17], who measured the nasal resistance in different configurations to identify possible sources of systematic bias in experimental measurements. In the present work, we focus on the case that more closely reproduced the active anterior rhinomanometry, which is illustrated in Fig. 2. In the clinical

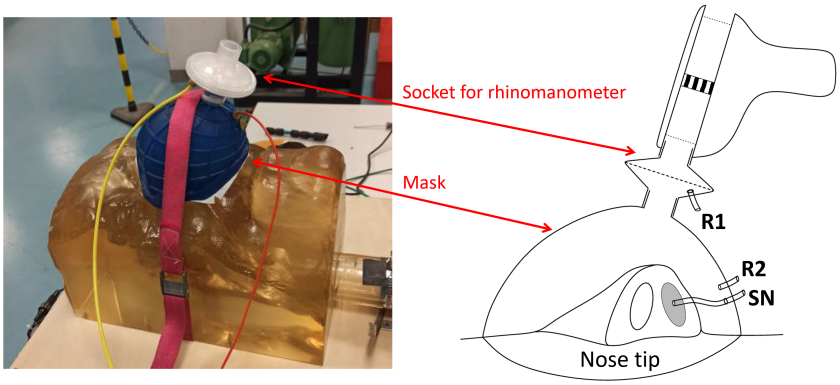

Figure 2: Photo and explanatory sketch of the experimental setup used by Tesa [17].

exam, patients wear a mask that completely covers the nose, they breath through the rhinomanometer, and one nostril is sealed. The flow rate, Q, is measured directly in the instrument, which also takes contemporaneous pressure measurements from two channels: the first pressure probe is inserted in the sealing of the sealed nostril, and the second is typically situated in the socket connecting mask and rhinomanometer. The locations of these two

probes are denoted by SN and R1 in Fig. 2, respectively. Note that the flow is approximately at rest in the portion of the nasal cavity corresponding to the sealed nostril, so that probe SN is capable of measuring the pressure up to the nasopharynx. The nasal resistance is then computed, for the side of the nasal cavity of the active nostril, as:

$$R = \frac{\Delta P}{Q} = \frac{P_{\mathrm{SN}} - P_{\mathrm{R1}}}{Q} \,. \tag{3}$$

In the complete medical exam, this procedure is then repeated for the inverting sealed and active nostrils, and the total nasal resistance is defined as that of the two branches in parallel:

$$R_{\mathrm{tot}} = \frac{R_{\mathrm{left}} R_{\mathrm{right}}}{R_{\mathrm{left}} + R_{\mathrm{right}}} \,. \tag{4}$$

We will focus on measures of R for the right nostril in this study. In the experimental setup, an additional pressure measurement is also taken with a probe inserted directly in the mask, at the location denoted by R2 in Fig. 2. This measure is taken as an alternative reference pressure with respect to R1. The other configurations of the experiments in Ref. [17] were designed to allow an estimate of the uncertainty of the fluxmeter and pressure probes in a rhinomanometer for clinical use, and are not considered in the present study. The errors intrinsic to the instruments have been found to be much lower than that associated with the choice of R2 over R1 for the reference pressure.

2.2. RANS Setup

RANS simulations are carried out with the open-source software OpenFOAM, which consists of a set of C++ libraries for the numerical solution of partial differential equation on unstructured grids with the finite-volume method [23]. The OpenFOAM solver for incompressible steady-state cases is *simpleFoam*, which is based on the semi-implicit method for pressure-linked equations (SIMPLE) algorithm. The turbulent model used for all simulations is the $k-\omega$ SST [24], used in its standard formulation as implemented in the code.

The internal nose is particularly complex and cannot realistically be described without relaying on automatic software for meshing, at least for codes for which the grid needs to perfectly adhere to the anatomical surface. For these RANS simulations, the grid is created using the two dedicated utilities provided by OpenFOAM, *blockMesh* and *snappyHexMesh*. The former can create structured grids from a given set of elementary geometrical shapes and cell sizes. The latter can create unstructured grids based on structured grids that are deformed to follow a set of surfaces (provided *e.g.* in *.stl* format),

and to which is possible to apply subsequent levels of refinement or adding layers parallel to the wall. The refinements for the second utility are typically prescribed in relative terms with respect to the underlining structure grid. It naturally follows from this procedure that a better resolution can be obtained both improving the resolution of the structured grid in the first step of the creation of the mesh (with *blockMesh*), or acting on refinement levels in the second step (using *snappyHexMesh*). The nature of the flow within the nasal cavity, which is fully three-dimensional and does not exhibit a developed boundary layer in the canonical sense, makes the creation of multiple layers of cells parallel to the wall potentially counter productive. For this reason, the set of 3 meshes required for a complete grid-dependency study has been created establishing a fixed number of refinement levels in the proximity of the wall (without creating a boundary-layer mesh) and acting only the resolution of the underlying structured grid.

The grid quality has been assessed using the standard criteria of maximum non-orthogonality, aspect ratio, and skewness, evaluated by the OpenFOAM utility *checkMesh* as follows: non-orthogonality is the angle defined between the line passing for the centres of two adjacent cells and the normal of face shared by the cells; skewness is the distance between the centre of the common face and the line between the cell centres of two adjacent cells; and aspect ratio is defined as:

$$AR = \frac{1.0}{6.0} \times \frac{|ax| + |ay| + |az}{V^{\frac{2.0}{3.0}}}, \tag{5}$$

where ax, ay, az are the areas of the sections of the cell bounding box in the three direction and V is the volume of the cell. These parameters are reported in Table 1, together with the number of cell in each grids, and sagittal sections at a select location within the active nostril are shown in Fig. 3.

Table 1: Quality parameters for three grids employed in RANS simulations

Notation	$2.2M$	$4.2M$	$5.9M$
Non-orthogonality	52.96°	53.35°	54.58°
Aspect Ratio	5.45	5.78	5.84
Skewness	2.094	2.098	2.098
Hexahedral %	86.38	86.95	87.3
# of grid points	$2,661,075$	$4,218,567$	$5,902,773$

Compromises in the choice of order of accuracy are often made in RANS simulations of complex geometries, to assure numerical convergence. For a proper estimate of the average pressure drop and flow rates through the nasal cavities, however, Schillaci & Quadrio [16] reported that using first-order

(a) Mesh $2.2M$ (b) Mesh $5.9M$

Figure 3: Portion of a sagittal section of the RANS grids with lowest and highest resolution.

numerical schemes for RANS is even more detrimental than using RANS over LES. In the present project, second-order numerical schemes have been used for the grid-dependency study, and one additional set of simulations on a selected grid have been carried out with first-order discretization of the advection term of all transport equations. The latter set of cases is considered to provide additional indications of the order of magnitude of uncertainties in RANS simulations. To increase stability, relaxation factors of 0.3 and 0.7 are chosen for the pressure and all other variables, respectively.

As stated above, only inspiration with different values of constant flow rates are considered. The spherical surface added in front of the model is treated as an inlet with imposed volumetric flow rate and a horizontal section of the trachea is the outlet. The volumetric flow rate is defined as a velocity inlet condition with a fixed density value of $\rho = 1.225$ $[kg/m^3]$ and a range of $200 - 600$ ml/s is considered. For the pressure, p, and turbulence viscosity, ν_t, a zero-gradient condition is imposed at the inlet; for the turbulence kinetic energy, k, a turbulence intensity of 1% is set and for the turbulent specific dissipation rate, ω, a value of 1 is imposed. At the outlet surface, on the other hand, velocity, k, ν_t, and ω are set with zero-gradient conditions. Additionally, a total-pressure condition with a value of zero is defined. This condition determines the outlet pressure based on the sign of the normal velocity to the outlet patch, which is the vertical velocity component in this case, u_z. When the sign of u_z is greater than or equal to zero, the static pressure is set to the defined value. Conversely, when u_z is less than zero, the total pressure is set to the specified value, and the static pressure is calculated as the difference between total and kinematic pressure. This correction effect contributes to achieving a stable solution. The surfaces of the nasal passageways are considered as solid wall and no-slip and no-penetration boundary conditions are applied. The boundary conditions are summarized in table 2.

Table 2: Summary of the boundary conditions in RANS simulations.

	Sphere	Head (Wall)	Outlet
u	$200 - 600\, cm^3/s$	0.0	zero-gradient
p	zero-gradient	zero-gradient	Total Pressure $= 0.0\, Pa$
ω	1.0	1.0	zero-gradient
ν_t	zero-gradient	0.0	zero-gradient
k	1%	10^{-10}	zero-gradient
ρ	$1.225\, kg/m^3$	-	-

Residual convergence for these simulations can be challenging to obtain, due to the low-Reynolds number instabilities in the pharynx and, as will be described in Section 3, the occurrence of separation just above the outlet. Simulations with dissipative schemes easily reached convergence in the traditional sense, with residuals for the three components of the momentum equation of the order of 10^{-7} after ≈ 600 iterations. Simulations with second-order discretization tend to converge with residuals for the velocity components at approximately 10^{-4}. These relatively high values of the residuals have been considered acceptable after verifying that the quantities of interest had oscillations of a similar magnitude, and thus much smaller than the mismatch under investigation.

2.3. DNS Setup

All direct numerical simulations have been run as a separate part of the project [25], while the post processing of the data was part of the present effort. These simulations are carried out using an in-house code based on the immersed-boundary method (IBM) described by Luchini [26] and written in the CPL programming language [27]. A previous version of the same code has been used by Vecchietti [15], in a systematic comparison with OpenFOAM. In the DNS code, the incompressible Navier-Stokes equations are discretized on a staggered Cartesian uniform grid using the second-order finite-difference approximation for all spatial derivative. A fractional step method and a third-order Runge-Kutta schemes are used for the time integration. The same computational domain described for the RANS simulations in the previous section is used in the DNSs, but the flow is driven imposing a fixed pressure difference between the external sphere and the outlet at trachea. For both surfaces, a zero-gradient conditions is imposed for the velocity. Four different resolutions are employed for these simulations, as summarized in Table 3, with the one at highest resolution having a total of $\approx 114 \cdot 10^6$ grid points within the region of domain that contains air.

In all cases, flow statistics are sampled for $1s$ of physical time after the

Table 3: Grids used in the DNS grid-dependency analysis.

Notation	$\Delta\tilde{x}$ [mm]	N_{tot}	N_{act}
$13M$	0.68	$65 \cdot 10^6$	$13 \cdot 10^6$
$25M$	0.54	$126 \cdot 10^6$	$25 \cdot 10^6$
$51M$	0.43	$256 \cdot 10^6$	$51 \cdot 10^6$
$114M$	0.32	$588 \cdot 10^6$	$114 \cdot 10^6$

initial transient is passed, which is assessed monitoring the time evolution of the flow rate across the outlet.

3. Results

In this section, the results of RANS simulations and DNS are presented, to describe the main features of the flow through the nasal cavity and to assess the order of magnitude of the errors that is reasonable to expect in these numerical simulations. Moreover, a comparison with experimental results extracted from Tesa [17] is carried out, to explain which source of error is compatible with the mismatch reported in the literature between CFD and clinical measurements of nasal resistance.

3.1. Numerical simulations

We begin with a qualitative comparison between RANS and DNS results. Fig. 4 shows a sagittal sections of the nasal cavity simulated with the two methodologies, for a similar flow rate of approximately $Q \approx 400 cm^3/s$, and with an intermediate resolution for both. To provide some indications of the flow behaviour, two physical quantities are considered: the mean-velocity magnitude, denoted with $\overline{u}_{\text{mag}}$, and the turbulent kinetic energy, denoted with k. Note that k is computed directly in the DNS from the three diagonal components of the Reynolds-stress tensor, *i.e.* $k = \frac{1}{2}(\overline{u'^2} + \overline{v'^2} + \overline{w'^2})$, and as a model variable in RANS simulations using the $k-\omega$ SST model. The mean velocity field is in good agreement between DNS and RANS simulations. In the nasal cavity, the flow is accelerated in where cross sections are smaller, preventing transition from a steady to an unsteady regime. Non-negligible fluctuations are observed in the nasopharynx, there the passageways are larger, and in the pharynx, where are most likely connected to the instability of a separation bubble. It is worth mentioning that an unsteady regime will naturally arise in the nasal cavity for more realistic inflow conditions, aiming at reproducing inhalation or exhalation [28], but not in the present case.

RANS simulations tend to predict a lower value of k then DNS, where

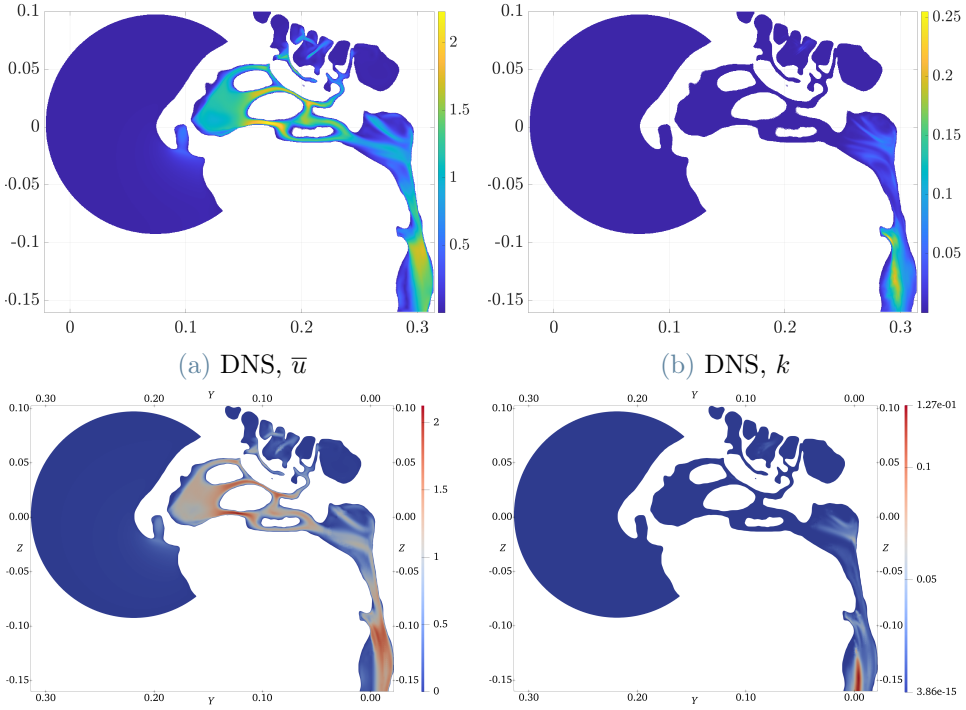

(a) DNS, $\overline{u}$ (b) DNS, k

(c) RANS, $\overline{u}$ (d) RANS, k

Figure 4: Selected sagittal sections of domain, showing the magnitude of mean velocity and turbulent kinetic energy for DNS($51M$) and RANS($4.2M$), for cases with a similar flow rate of $Q \approx 400cm^3/s$.

k is non-negligible (note however that there is no direct correspondence between the model variable k and the turbulent kinetic energy computed from statistics in a DNS, and a comparison between the two is not particularly informative). The fact that both RANS and DNS predict a steady laminar flow in the region of interest still holds true for the higher flow rates considered in this study (not shown here) and it is an encouraging result suggesting that the overall uncertainty of numerical simulations should be reasonably low.

Together with the total flow rate, pressure measurements are necessary to compute the nasal resistance. We now examine pressure values sampled at five locations in the computational domain and for the two simulations considered above, to describe where the relevant pressure drops occur. The probe locations are shown in Fig. 5. Locations P1 and P2 are both within

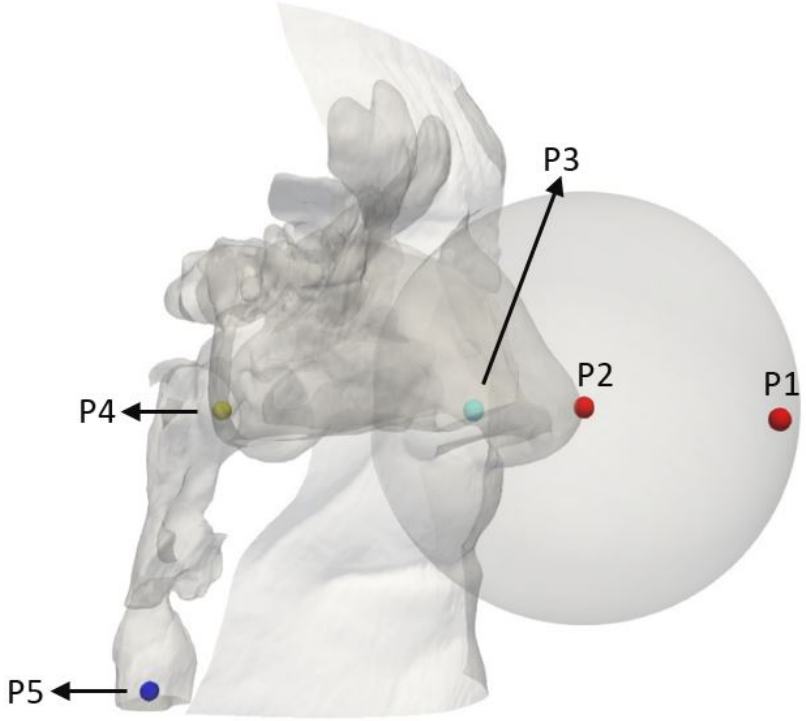

Figure 5: Locations of the pressure probe in the computational domain.

the spherical shape that is supposed to represent an inner portion of the space enclosed within the mask in experiments (and clinical measurements). The flow is almost at rest in this region of the domain, so both locations are supposed to have the same pressure values and are equivalent to the reference pressure probe denoted with R2 in the experiment. Location P3, which is on the interior surface of the sealing of the sealed nostril, is directly equivalent to probe SN in the experiment. Location P4 is in the nasopharynx, and

it is considered here to confirm that the pressure at this location is the same as measured in P3 (or SN). Location P5, at the outlet, provides here a reference pressure value to enable a direct comparison between DNS and RANS (which have different absolute pressure values). The pressure values are reported in Table 4. Note that, as mentioned above, the flow is considered as incompressible and both RANS and DNS calculate the kinematic pressure. The pressure is then multiply with the air density in standard conditions ($1.225kg/m^3$) and expressed in Pascal (Pa).

Table 4: Pressure values for RANS($4.2M$) and DNS($51M$), in Pascal (Pa).

Probe	Location in Geometry	RANS($4.2M$)	DNS($51M$)
P1 (-P5)	Sphere frontal extreme	6.147	6.169
P2 (-P5)	Sphere centre	6.146	6.168
P3 (-P5)	Interior sealed nostril	2.132	2.027
P4 (-P5)	Nasopharynx	2.115	1.998
P5 (-P5)	Trachea	0	0

As expected, pressure values in P1 and P2 are virtually identically and those in P3 and P4 differ from $\approx 1\%$. This first quantitative comparison between RANS and DNS also confirm the previous qualitative observation that the two methodologies give results in good agreement.

We now focus on the effects of resolution and choice of numerical schemes, which are assessed comparing $\Delta P = P_{\mathrm{P3}} - P_{\mathrm{P1}}$ as a function of Q for both DNS and RANS data sets. For the RANS simulations, for which a range of flow rates between $200cm^3/s$ and $600cm^3/s$ is considered, the results are shown in Fig. 6. As reported in Ref. [16], the choice of first-order numerical schemes, in this case just for the advection terms of the governing equations, has a much higher impact on RANS results than that of the resolutions. As expected, using lower-order numerical schemes, with higher numerical dissipation, results in a higher pressure drop when the same total flow rate is imposed. A change of resolution for the cases with full second-order discretization has a much smaller effect. Interestingly, improving the resolution also causes an increase of ΔP, in the same direction as a reduction of the order of accuracy, which is low but consistent for all cases. This apparently counter-intuitive finding can be explained by the fact that the leading source of numerical errors is no longer related to an excess of numerical dissipation. The fact that the discrepancy between different grids increases with the flow rates may suggest that this behaviour is related to the model sensitivity in regions with complex non-stationary flow, beyond the nasal cavity (this hypothesis has not been further investigated because the discrepancy is negligible if compared against all other source of errors discussed in this study). Another, perhaps unexpected, observation is that such small mismatch be-

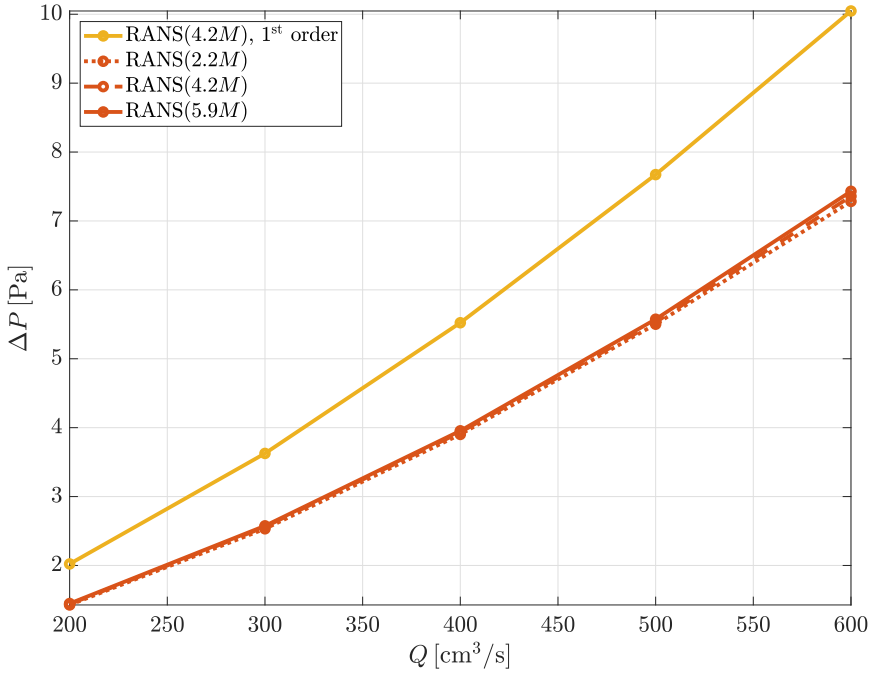

Figure 6: Pressure drop in the nasal cavity as a function of flow rate for RANS simulations.

tween RANS results for different resolutions is found for grids that are not using particular small cell sizes, if compared against those commonly used in the literature. To the contrary, the coarser grid that is considered here has a much lower number of cells than that typically assumed adequate in the literature.

The effects of increasing resolution for the IMB DNS code are shown in Fig. 7. To reduce the computational cost of the study, the grid-dependency analysis carried out for the DNS data set is more limited than that for the RANS simulations, which is considered an acceptable compromise because the aim of the present study is only to provide a general estimate of the errors that is reasonable to expect for these simulations. In these circumstances, it is not necessary to demonstrate that a fully-resolved DNS has been carried out for each flow rate. Simulations are then carried out for a range of flow rates between approximately $Q = 150cm^3/s$ and $500cm^3/s$ for the coarsest grid, G1, and an intermediate one, G3, and using all four grids only for cases with $Q \approx 400cm^3/s$. To examine these results, it is important to note that, since the flow is driven by a fixed pressure difference between spherical inlet and trachea outlet, a change of resolution affect both the total flow rates and ΔP between P1 and P3. This fact, which is fully apparent for the four cases at $Q \approx 400cm^3/s$, causes the data points in a ΔP vs Q plot to move along an oblique trajectory, rather than a vertical line. In other words, all

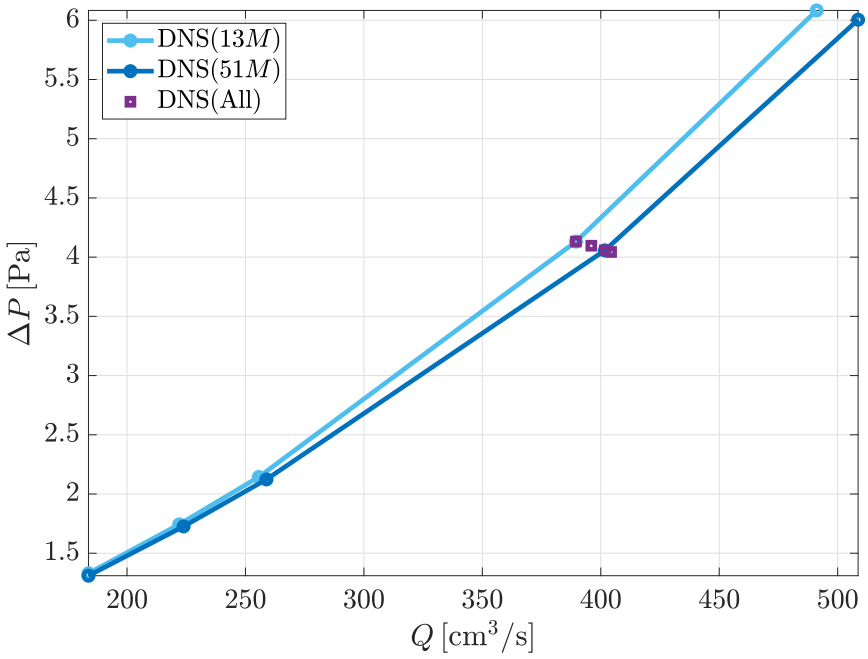

Figure 7: Pressure drop in the nasal cavity as a function of flow rate for DNSs.

following variables are changed: the pressure drops corresponding to the two portions of domain upstream and downstream the nasopharynx, their ratio, and the flow rate. Two additional points should be taken into account as well in the interpretation of this plot. Firstly, the change of resolution slightly modify the geometry, because it also has an impact on the IMB correction, which can potentially be more significant than expected given the relatively narrow sections of the nasal cavity. Secondly, no sub-grid model or other form of regularizations are implemented in the code.

In these circumstances, it is difficult to formulate a robust interpretation of the two main trends observed in the grid-dependency analysis, which are that a lower resolution causes an increase of resistance, and this increase is progressively more pronounced at higher flow rates. It is nonetheless possible to state that the coarsest grid, G1, is clearly not sufficient for a fully-resolved simulation, which is evident from the mismatch between results obtain for G1 and G3 at $Q \approx 500 cm^3/s$, and that this mismatch gives an indication of the possible uncertainty caused by lack of resolution in a direct numerical simulations.

We now go back to consider together the results for RANS and DNS. Fig. 8 shows the subset of both data sets in the proximity of $Q = 400 cm^3/s$, where we have available the full grid-dependency study for the two methodologies. Significantly, there are good indications that both RANS and DNS

are converging towards the same ΔP vs Q curve. This finding indicates that the good agreement between both methodologies is not an accident, and corroborates our assumption that is possible to use the mismatch between different cases in our numerical data set as a more general indication for the reasonable errors that should be excepted in simulations.

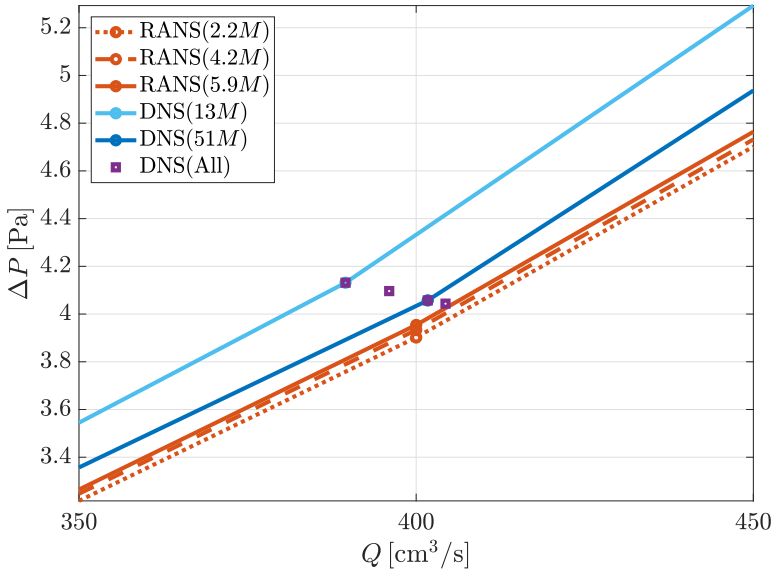

Figure 8: Comparison between DNS and RANS simulations for a subset of the data set.

3.2. Comparison with experiments

We now expand the considered data set including the experimental results for the configurations corresponding to that in the numerical simulations described above. Firstly, we focus on a comparison for ΔP vs Q, as done for the grid-dependency analysis in the previous section, which is shown in Fig. 9. For the experiments, we include results both for the pressure drop computed using the standard reference pressure in rhinomanometers, *i.e.*:

$$\Delta P_{\mathrm{R1}} = P_{\mathrm{R1}} - P_{\mathrm{SN}}\,, \tag{6}$$

and using as reference pressure the measure within the space enclosed by the mask, meaning:

$$\Delta P_{\mathrm{R2}} = P_{\mathrm{R2}} - P_{\mathrm{SN}}\,. \tag{7}$$

From a qualitative point of view, it is immediately apparent that the choice of reference pressure has an dramatic impact on the values of ΔP. The mismatch between the two experimental curves is, in fact, much larger than that

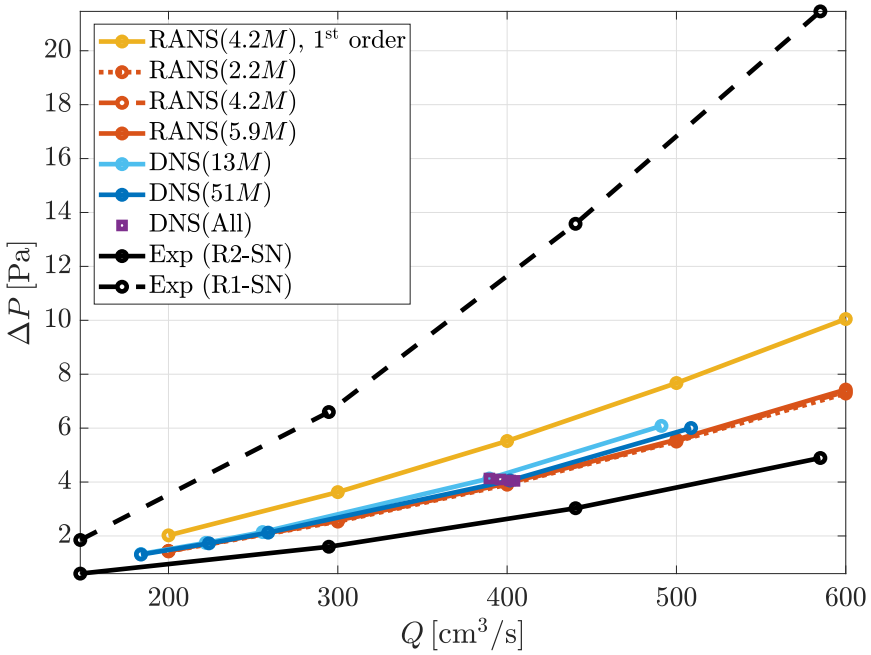

Figure 9: Pressure drop in the nasal cavity as a function of flow rate for all cases considered in the present study.

between any of the numerical simulations considered in the present study, even for DNS and RANS simulations with dissipative numerical schemes. Unfortunately, it also appears that the curve ΔP vs Q to which the simulations are converging is not any of the experimental ones, but it is closer to that for ΔP_{R2}. The observation that ΔP_{R1} is much higher than ΔP_{R2} can be readily explained by the fact that the position of the pressure probe within the socket connecting mask and rhinomanometry causes an additional resistance to be consider in the measurement, which is not negligible with respect to that of the nasal cavity (this was the core result presented in Ref. [17]). This bias cannot be simply explained with the resistance of the cylindrical duct departing from the mask, which has a cross-section quite larger than that typical in the nasal cavity, but is most likely related to the design of the socket where the measure takes place.

We can finally provide a quantitative evaluation of the discrepancies on the main quantity of interest, which is the nasal resistance. Consistently with the AAR procedure, R is computed in all simulations as:

$$R = \frac{P_{\mathrm{P3}} - P_{\mathrm{P1}}}{Q}\,, \tag{8}$$

and, in the experiments, with both ΔP_{R1} and ΔP_{R2}. We focus on the value of estimated nasal resistance for a flow rate of $Q = 400 cm^3/s$ and we take

the case DNS2 as reference. The relative error is then computed as:

$$\frac{\Delta R_{\mathrm{X}}}{R} = \frac{R_{\mathrm{X}} - R_{\mathrm{DNS}(51M)}}{R_{\mathrm{DNS}(51M)}} \,. \tag{9}$$

Note that, since the data set is not created for matching values of Q or ΔP, interpolation is required to obtain the estimated R at a given Q for all cases. The associated uncertainty in the interpolation is negligible with respect to the other sources of error, given that ΔP as a function of Q is necessary a regular function (and that $Q = 400 cm^3/s$ is an intermediate value in for all available data sets). The relative errors are reported for a select sample of cases in Table 5. As expected, given the previous results

Table 5: Relative error on the nasal resistance for $Q = 400$ cm^3/s, assuming DNS($51M$) as a reference.

Source of error under scrutiny	Cases	$\Delta R/R$
Lack of resolution in DNS	DNS($13M$)-DNS($51M$)	7%
Numerical dissipation in RANS	RANS($4.2M$), 1$^{\mathrm{st}}$ order-DNS($51M$)	37%
Resolution & modelling in RANS	RANS($2.2M$)-DNS($51M$)	-3%
Resolution & modelling in RANS	RANS($5.9M$)-DNS($51M$)	-2%
Experiment with clinical set up	Exp(R1)-DNS($51M$)	185%
Experiment with alternative set up	Exp(R2)-DNS($51M$)	-36%

on ΔP, the main cause of uncertainty is found to be, by far, the choice of measurement of reference pressure, which is also compatible with the large mismatch in the literature. Furthermore, all other sources of error are shown to have a lower impact on the value of R, quite lower than what would be necessary to explain the discrepancy observed in previous work.

4. Conclusions

A new data set of numerical simulations has been created to investigate the mismatch between CFD and clinical measurements of nasal resistance, which is complementary to a previous experimental campaign. These experiments provided an estimate of the possible bias caused in clinical instruments by the position of the probe that samples the reference pressure necessary to compute the nasal resistance. The simulations carried out in the present study were designed to replicate the setup of a sub set of the experiments, where an alternative definition of the reference pressure was adopted. Our results, even though are not in excellent agreement with those of the experiments in the configuration that we aimed to reproduce, are closer to those with that setup than to the experiment replicating standard clinical

measurements. This conclusion is reached for both DNS and RANS simulations, regardless of whether a grid with insufficient resolution or dissipative numerical schemes were used. Furthermore, the largest discrepancy between numerical simulations are much lower than the discrepancy arising in the experiments if the definition of the reference pressure is changed. Lastly, the discrepancy between numerical simulations are not high enough to justify the mismatch reported in the literature between clinical rhinomanometry and CFD, but those caused by a changed of reference pressure in the experiments are. Our results thus indicate a potential flaw in the design of rhinomanometers, and that this source of biased is probably responsible for the difficulties in reproducing clinical measurements with CFD.

We recognize that the present study may suffer from the following limitations. Since the experiments were based on the design of one medical instrument, it is possible that the bias that was measured is lower in other devices. It needs to be mentioned however that most rhinomanometers, by visual inspection of the different models in use nowadays, tend to have a similar position of the pressure probes. For this reason, we think that the lack of generality from this point of view should not be a critical issue. The usage of significant simplifications in the flow conditions may also have some impact on our results. It is possible, for instance, that a lack of resolution may cause larger numerical errors if a time-dependent input is considered, which would include a peak of flow rate higher than the mean. Lastly, the relatively poor agreement between experiment and simulations, with respect to the low uncertainty of the latter, still ought to be fully addressed.

References

[1] J. S. Rhee, D. T. Book, M. Burzynski, and T. L. Smith. "Quality of Life Assessment in Nasal Airway Obstruction". *The Laryngoscope* **113** (7) (2003), 1118–1122.

[2] K. Vogt, A. A. Jalowayski, W. Althaus, C. Cao, D. M. Han, W. Hasse, H. Hoffrichter, R. Mösges, J. F. Pallanch, K. Shah-Hosseini, K. Peksis, K. Wernecke, L. T. Zhang, and P. Zaporoshenko. "4-Phase-Rhinomanometry (4PR)–basics and practice 2010." *Rhinology. Supplement* **21** (2010), 1–50.

[3] H. Thulesius. "Rhinomanometry in clinical use. A tool in the septoplasty decision making process." PhD thesis. Lund University, 2012.

[4] M. Berger, M. Pillei, A. Giotakis, A. Mehrle, W. Recheis, F. Kral, M. Kraxner, H. Riechelmann, and W. Freysinger. "Pre-surgery planning tool for estimation of resection volume to improve nasal breathing based on lattice Boltzmann fluid flow simulations". *Int J CARS* **16** (4) (2021), 567–578.

[5] M. Quadrio, C. Pipolo, S. Corti, R. Lenzi, F. Messina, C. Pesci, and G. Felisati. "Review of computational fluid dynamics in the assessment of nasal air flow and analysis of its limitations". *Eur Arch Otorhinolaryngol* **271** (9) (2014), 2349–2354.

[6] T. Radulesco, L. Meister, G. Bouchet, J. Giordano, P. Dessi, P. Perrier, and J. Michel. "Functional relevance of computational fluid dynamics in the field of nasal obstruction: A literature review". *Clinical Otolaryngology* **44** (5) (2019), 801–809.

[7] J. Kimbell, G. Garcia, D. Frank, D. Cannon, S. Pawar, and J. Rhee. "Computed nasal resistance compared with patient-reported symptoms in surgically treated nasal airway passages: A preliminary report". *Am. J. Rhinology \& Allergy* **26** (3) (2012), e94–e98.

[8] J. Osman, F. Großmann, K. Brosien, U. Kertzscher, L. Goubergrits, and T. Hildebrandt. "Assessment of nasal resistance using computational fluid dynamics". *Current Directions in Biomedical Engineering* **2** (1) (2016), 617–621.

[9] K. Vogt, K.-D. Wernecke, H. Behrbohm, W. Gubisch, and M. Argale. "Four-phase rhinomanometry: a multicentric retrospective analysis of 36,563 clinical measurements". *European Archives of Oto-Rhino-Laryngology* **273** (5) (2016), 1185–1198.

[10] M. Berger, A. Giotakis, M. Pillei, A. Mehrle, M. Kraxner, F. Kral, W. Recheis, H. Riechelmann, and W. Freysinger. "Agreement between rhinomanometry and computed tomography-based computational fluid dynamics". *Int J CARS* (2021).

[11] M. Berger, M. Pillei, A. Mehrle, W. Recheis, F. Kral, M. Kraxner, Z. Bardosi, and W. Freysinger. "Nasal cavity airflow: Comparing laser doppler anemometry and computational fluid dynamic simulations". *Respiratory Physiology & Neurobiology* **283** (2021), 103533.

[12] N. Schmidt, H. Behrbohm, L. Goubergrits, T. Hildebrandt, and J. Brüning. "Comparison of rhinomanometric and computational fluid dynamic assessment of nasal resistance with respect to measurement accuracy". *Int J CARS* (2022).

[13] M. Waldmann, A. Grosch, C. Witzler, M. Lehner, O. Benda, W. Koch, K. Vogt, C. Kohn, W. Schröder, J. H. Göbbert, and A. Lintermann. "An effective simulation- andmeasurement-based workflow for enhanced diagnostics in rhinology". *Medical & Biological Engineering & Computing* (Issue 2/2022) (2021).

[14] K. Karbowski, B. Kopiczak, R. Chrzan, J. Gawlik, and J. Szaleniec. "Accuracy of virtual rhinomanometry". *Polish Journal of Medical Physics and Engineering* **29** (1) (2023), 59–72.

[15] L. Vecchietti. "A Direct Numerical Simulation code for the flow in the human nose". PhD thesis. Politecnico di Milano, 2021.

[16] A. Schillaci and M. Quadrio. "Importance of the numerical schemes in the CFD of the human nose". *Journal of Biomechanics* **138** (2022), 111100.

[17] G. Tesa. *Rinomanometria: uno studio teorico-sperimentale*. Politecnico di Milano, https://hdl.handle.net/10589/205304. 2023.

[18] R. Tjahjono and N. Singh. "Correlation between nasal mucosal temperature change and the perception of nasal patency: a literature review". *The Journal of Laryngology & Otology* **135** (2) (2021), 104–109.

[19] R. Tjahjono, H. Salati, K. Inthavong, and N. Singh. "Correlation of Nasal Mucosal Temperature and Nasal Patency—A Computational Fluid Dynamics Study". *The Laryngoscope* **n/a** (n/a) (2022).

[20] I. R. Cal, J. L. Cercos-Pita, and D. Duque. "The incompressibility assumption in computational simulations of nasal airflow". *Computer Methods in Biomechanics and Biomedical Engineering* **20** (8) (2017), 853–868.

[21] I. Hörschler, W. Schröder, and M. Meinke. "On the assumption of steadiness of nasal cavity flow". *Biomechanics* **43** (2010), 1081–1085.

[22] H. Calmet, A. Gambaruto, A. Bates, M. Vázquez, G. Houzeaux, and D. Doorly. "Large-scale CFD simulations of the transitional and turbulent regime for the large human airways during rapid inhalation". *Comp. Biol. Med.* **69** (2016), 166–180.

[23] H. Weller, G. Tabor, H. Jasak, and C. Fureby. "A tensorial approach to computational continuum mechanics using object-oriented techniques". *Computers in Physics* **12** (6) (1998), 620–631.

[24] F. R. Menter, M Kuntz, and R Langtry. "Ten Years of Industrial Experience with the SST Turbulence Model". *Turbulence, Heat and Mass Tansfer*. Turbulence, Heat and Mass Tansfer **4** (2003), 8.

[25] M. Atzori and M. Quadrio. *DNS of the nasal cavity*. Private Communication. 2023.

[26] P. Luchini. "Immersed-boundary simulation of turbulent flow past a sinusoidally undulated river bottom". *Eur. J. Mech. B / Fluids* **55** (2016), 340–347.

[27] P. Luchini. *Introducing CPL*. arXiv:2012.12143. 2020.

[28] H. Calmet, K. Inthavong, H. Owen, D. Dosimont, O. Lehmkuhl, G. Houzeaux, and M. Vázquez. "Computational modelling of nasal respiratory flow". *Computer Methods in Biomechanics and Biomedical Engineering* **24** (4) (2021), 440–458.

Abstract in lingua italiana

È stata spesso osservata una significativa discrepanza tra misure cliniche di resistenza nasale e risultati di simulazioni numeriche, discrepanza maggiore di quella realisticamente attribuibile alle incertezze di apparati sperimentali o errori numerici. Lo scopo di questo lavoro è identificare possibili cause di incertezza in questa misura che siano compatibili con le differenze osservate. A tal fine, i risultati di una precedente campagna sperimentale sono confrontati con quelli di simulazioni numeriche sulla stessa geometria, sia utilizzando modelli (simulazioni RANS) sia con soluzione diretta dell'equazione di Navier-Stokes (DNS). Esperimenti e simulazioni sono concepiti per riprodurre il metodo della più diffusa tecnica di rinomanometria. Di tutte le cause di incertezza analizzate, comprese una risoluzione insufficiente, l'uso di modelli o di schemi numerici con alta dissipazione, abbiamo determinato che la più alta è legata alla posizione delle misure di pressione negli strumenti usati nella pratica clinica. Questa possibile fonte di errore è anche l'unica compatibile con le differenze osservate tra misure e simulazioni. I nostri risultati suggeriscono che scelte di progettazione di molti strumenti per misure mediche abbiano introdotto una fonte di errori sistematici nella misura della resistenza nasale e che questi errori sistematici siano la causa principale delle differenze tra misure cliniche e simulazioni numeriche.

Parole chiave: Resistenza Nasale, Rinomanometria, CFD